Biochimica et Biophysica Acta 1822 (2012) 1258–1269

Contents lists available at SciVerse ScienceDirect

Biochimica et Biophysica Acta

journal homepage: www.elsevier.com/locate/bbadis

Targeted knockdown of *Cerkl*, a retinal dystrophy gene, causes mild affectation of the retinal ganglion cell layer

Alejandro Garanto [a,b,c], Javier Vicente-Tejedor [d], Marina Riera [a,b,c], Pedro de la Villa [d], Roser Gonzàlez-Duarte [a,b,c,*,1], Román Blanco [e,**,1], Gemma Marfany [a,b,c,***,1]

[a] *Departament de Genètica, Facultat de Biologia, Spain*
[b] *Institut de Biomedicina (IBUB), Universitat de Barcelona, Barcelona, Spain*
[c] *CIBERER, Instituto de Salud Carlos III, Barcelona, Spain*
[d] *Departamento de Fisiología, Facultad de Medicina, Universidad de Alcalá, Alcalá de Henares, Madrid, Spain*
[e] *Departamento de Cirugía, Facultad de Medicina, Universidad de Alcalá, Alcalá de Henares, Madrid, Spain*

ARTICLE INFO

Article history:
Received 18 November 2011
Received in revised form 10 April 2012
Accepted 11 April 2012
Available online 19 April 2012

Keywords:
Knockout model
Retinal dystrophy
Retinitis pigmentosa
Ganglion cell

ABSTRACT

In order to approach the function of the retinal dystrophy *CERKL* gene we generated a novel knockout mouse model by cre-mediated targeted deletion of the *Cerkl* first exon and proximal promoter. The excised genomic region (2.3 kb) encompassed the first *Cerkl* exon, upstream sequences including the proximal promoter and the initial segment of the first intron. The *Cerkl* −/− mice were viable and fertile. The targeted *Cerkl* deletion resulted in a knockdown more than a knockout model, given that alternative promoters (unreported at that time) directed basal expression of *Cerkl* (35%). *In situ* hybridizations and immunohistochemistry showed that this remnant expression was moderate in the photoreceptors and weak in the ganglion and inner cell layers. Morphological characterization of the *Cerkl* −/− retinas did not show any gross structural changes, even at 12 months of age. However, some clear and consistent signals of gliosis and retinal stress were detected by the statistically significant increase of i) the glial fibrillary antigen protein (GFAP) expression, and ii) apoptosis, as detected by TUNEL. Remarkably, consistent non-progressive perturbation (from birth up to 12 months of age) of ganglion cells was supported by the decrease of the Brn3a marker expression as well as the reduced oscillatory potentials in the electroretinographic recordings. In conclusion, the *Cerkl* −/− knockdown shows a mild retinal phenotype, with increased levels of cellular stress and apoptosis indicators, and clear signs of functional alteration at the ganglion cell layer, but no detectable morphological changes.

1. Introduction

Mutations in the *CERKL* gene are associated to autosomal recessive retinal degeneration. First characterized as a Retinitis Pigmentosa (RP) causing gene [1–6], and later also considered to promote Cone-Rod Dystrophy (CRD) [7,8], its classification as a RP or CRD gene is still under question. In fact, although the association of *CERKL* mutations with retinal pathology is clear, we are still at the dark concerning its physiological function and contribution to the progressive photoreceptor degeneration.

CERKL [6] was named after the amino acid identity conservation with CERK [9], the reported ceramide kinase enzyme, known to phosphorylate the sphingolipid ceramide to ceramide-1-phosphate (C1P) [10], whose balance acts as cellular rheostat between apoptosis *versus* survival signaling pathways [11–13]. Although CERKL has an intact diacylglycerol kinase domain [6,14], no kinase activity neither on lipids nor proteins, could be assigned after intense studies from many groups [14–16]. Remarkably, overexpression of CERKL in cultured cells confers protection against apoptosis caused by oxidative stress injury, providing the first experimental clues on its role in retinal cell protection [16].

Very recently, an accurate assessment of the transcriptional products has unveiled that *CERKL* shows a high repertoire of transcript isoforms due to a combination of extensive alternative splicing plus the use of at least three additional promoters [17]. Adding to the complexity of CERKL functional analysis, the protein subcellular localization is extremely dynamic, shifting from the cytoplasm – where it mainly localizes associated to the endoplasmic reticulum and Golgi membranes – to the nucleus, and seldom at the nucleoli [16].

CERKL shows a wide tissular expression although the tissues where the expression is highest are retina in humans and retina and liver in mouse [17]. *In situ* mRNA hybridization on mouse retinal sections showed strong *Cerkl* specific expression in the ganglion cell layer (GCL), moderate and interspersed staining in the inner nuclear layer (INL), and

* Corresponding author. Tel.: +34 934021034.
** Corresponding author. Tel.: +34 918854522.
*** Corresponding author. Tel.: +34 934021502.
E-mail addresses: rgonzalez@ub.edu (R. Gonzàlez-Duarte), roman.blanco@uah.es (R. Blanco), gmarfany@ub.edu (G. Marfany).
[1] These authors contributed equally to this work.

0925-4439/$ – see front matter © 2012 Elsevier B.V. All rights reserved.
doi:10.1016/j.bbadis.2012.04.004

faint detection in the inner segment of photoreceptors, whereas immunohistochemistry with antibodies against specific epitopes revealed strong CERKL colocalization with cones, fainter in rods, and moderate at the INL and GCL.

Our group first identified the R257X mutation in CERKL [6], which it is also the most frequent and accounts for more than half of the reported mutated alleles [17]. This mutation is located on exon 5, one of the alternatively spliced exons, and thus some but not all protein isoforms are compromised. To evaluate the phenotype of this mutation, a mouse model in which exon 5 had been excised was constructed [18]. The homozygous exon 5-deleted mice did not show any apparent phenotype in the retina.

In this context, to shed light on CERKL physiological role and the *in vivo* consequences of its mutations, we aimed to generate a full knockout *Cerkl*−/− mouse model by targeted deletion of the reported promoter and the first exon, according to the knowledge at that time. However, the use of alternative promoters driving residual transcription in the retina turned our knockout into a knockdown model retaining 30–35% of *Cerkl* mRNA isoforms, all of them lacking the first exon and initiating methionine. The homozygous exon 1-deleted *Cerkl*−/− mice show increased levels of retinal stress and apoptosis, and diminished expression of the ganglion cell marker Brn3a, but no gross morphological retinal alterations. Most interestingly, the electroretinographic changes observed in the oscillatory potential waveforms are in accordance with the reduced levels of *Cerkl* mRNA and Brn3a protein levels in the retina of the KO mice.

2. Material and methods

2.1. Animal handling, tissue dissection and preparation of samples

Murine tissue samples were obtained from *Cerkl*+/+ and *Cerkl*−/− C57BL/6J background mice. All procedures were performed according to ARVO statement for the use of animals in ophthalmic and vision research, as well as the regulations of the Animal Care facilities at the University of Barcelona. Animals were euthanized with CO_2 followed by cervical dislocation. Specific tissues and organs were dissected and immediately frozen in liquid nitrogen.

2.2. Generation of the knockout Cerkl −/− mouse model

The strategy, the generation of targeting constructs, initial ES cell screening, breeding, housekeeping and molecular genotyping of all the mice after the G0 generation as well as the crosses to obtain the knockout animal model have been performed in our lab. ES transfection, handling, and the generation of chimeric embryos for the obtention of the founder mouse *Cerkl*+/− were performed by GenOway (Lyon, France). A diagram of the targeted locus is depicted in Fig. 1A. In brief, the genomic sequences corresponding to the 5′ and 3′ flanking regions of the *Cerkl* promoter and exon 1 were amplified from 129/SvPas genomic DNA. These sequences were referred as long (region before exon 1) and short (intron 1) arms of homology (LA and SA). Several sub-cloning steps were performed to obtain the final targeting vector using pPCR-Script SK (+) vector (Stratagene). The first step consisted in the addition of a loxP site into LA. A synthetic exon 1 construct with new restriction sites (GeneArt) was used to clone the amplified SA fragment. A Neomycin resistance gene (NEO) flanked by two FRT and one loxP sites were also introduced into SA. Finally, both homology arms were cloned together and the negative selection cassette, DTA (Diphteria Toxin A), was added. The resulting targeting vector stretched 15384 bp, was fully validated by sequencing, and was electroporated into 129Sv ES cells. Positive selection was performed 24 h after electroporation by adding geneticin (200 μg/ml), and more than 1000 geneticin-resistant clones were isolated and amplified. After PCR screenings for recombination at the 5′ and 3′ flanking regions, a total of 14 clones were obtained. Those were characterized by Southern Blot using two different probes, 5′ probe and 3′ probe (Fig. 1B). Only 5 clones had recombined at the correct sites. ES positive cells were used for C57BL/6J blastocyst injections and led to the generation of 9 male chimeras displaying a chimerism rate ranging from 50 to 80%. Highly chimeric males (80% chimerism) were mated with C57BL/6J Flp-deleter females to allow the excision of the NEO selection cassette. Pups were genotyped, and those that presented the excision of the cassette were breeded with wild-type C57BL/6J. The first generation of floxed mice was obtained by mating 2 heterozygous floxed males with C57BL/6J Cre-deleter females to allow the germline excision of the floxed region. Mice were subsequently bred with C57BL/6J mice for a total of 5 generations and pups were genotyped by PCR from tail or ear samples.

2.3. Genotyping by Southern blot and PCR

Genomic DNA from ES cells growing after double positive–negative selection was obtained by standard protocols, after a mild lysis, overnight proteinase K digestion and nucleic acid precipitation with ethanol. Ten micrograms of DNA were digested with informative restriction enzymes, separated by agarose electrophoresis and transferred to Nylon membranes. Standard protocols for pre-hybridization, hybridization with ^{32}P-labeled probes (whose position is indicated in Fig. 1A) were used. Autoradiographic exposition and image acquisition were performed with BioRad Molecular Imager FX Pro Plus (Bio-Rad, Hercules, CA). Three PCR genotyping primers (Fw, Rv1 and Rv2, sequences in Table 1) were used at the same time to allow genotyping of the WT and the floxed alleles in a single reaction (Fig. 1D). The PCR reaction included a first denaturing step of 120 s at 94 °C, followed by 35 cycles of 94 °C for 20 s, 59 °C for 30 s, and 72 °C for 60 s.

2.4. RNA extraction and RT-PCRs

Twenty-five milligrams of each frozen mouse tissue were homogenized using a Polytron PT 1200 E homogenizer (Kinematica AG, Lucerne, Switzerland). For total RNA extraction, High Pure RNA Tissue Kit (Roche Diagnostics, Indianapolis, IN) was used, following the manufacturer's instructions. Total RNA was quantified using the nanoquant plate in an Infinite 200 microplate reader (Tecan, Männedorf, Switzerland).

The RT-PCR assay was carried out with the Transcriptor High Fidelity cDNA Synthesis Kit (Roche Diagnostics, Indianapolis, IN) performed following the manufacturer's protocol, using 200 ng of mouse total RNA. For tissue expression analysis all reaction mixtures (50 μl) contained 10 μM of each primer pair, 2 μM of dNTPs, 1.5 mM $MgCl_2$ and 1 U of Go*Taq* polymerase (Promega, Madison, WI). A pair of primers was used to amplify mouse *Gapdh* (Table 1) to compare and normalize the samples. Two-step PCR conditions were as follows: 120 s at 94 °C and 30 cycles of 94 °C for 20 s and 63 °C for 120 s. Mouse *Cerkl* expression was detected with primers mRT_F and mRT_R (a first denaturing step of 120 s at 94 °C, followed by 35 cycles of 94 °C for 20 s, 60 °C for 30 s, and a final extension step at 72 °C for 20 s). The characterization of the different alternative promoters was performed on cDNAs using a forward primer located in each promoter (NeuroD1_F, UTR_F, 3a_F and 3b_F) and the same reverse primer in exon 12 mRT_R (Table 1). Primers were designed to share the melting temperatures and optimized for the same amplification conditions: 120 s at 94 °C followed by 40 cycles of 94 °C for 20 s, 58 °C for 30 s and 72 °C for 90 s. Oligonucleotide sequences are listed in Table 1 and their localization is depicted in Supplementary Fig. 1.

Real-time PCR was performed using the SYBR Green I Master assay in a LightCycler480 (Roche, Indianapolis, IN). Specific primers in different exons were designed to generate an amplicon of approximately 100 bp. Oligonucleotide sequences are listed in Table 1. The expression of *β-2-microglobulin* was used for normalization and comparison to *Brn3a* and *Gfap* target genes. For each real-time PCR reaction, 2 μl of cDNA (diluted 1:5), 1 μM of each primer, 1× master mix and H_2O were mixed in a final volume of 10 μl. The reaction was pre-incubated for

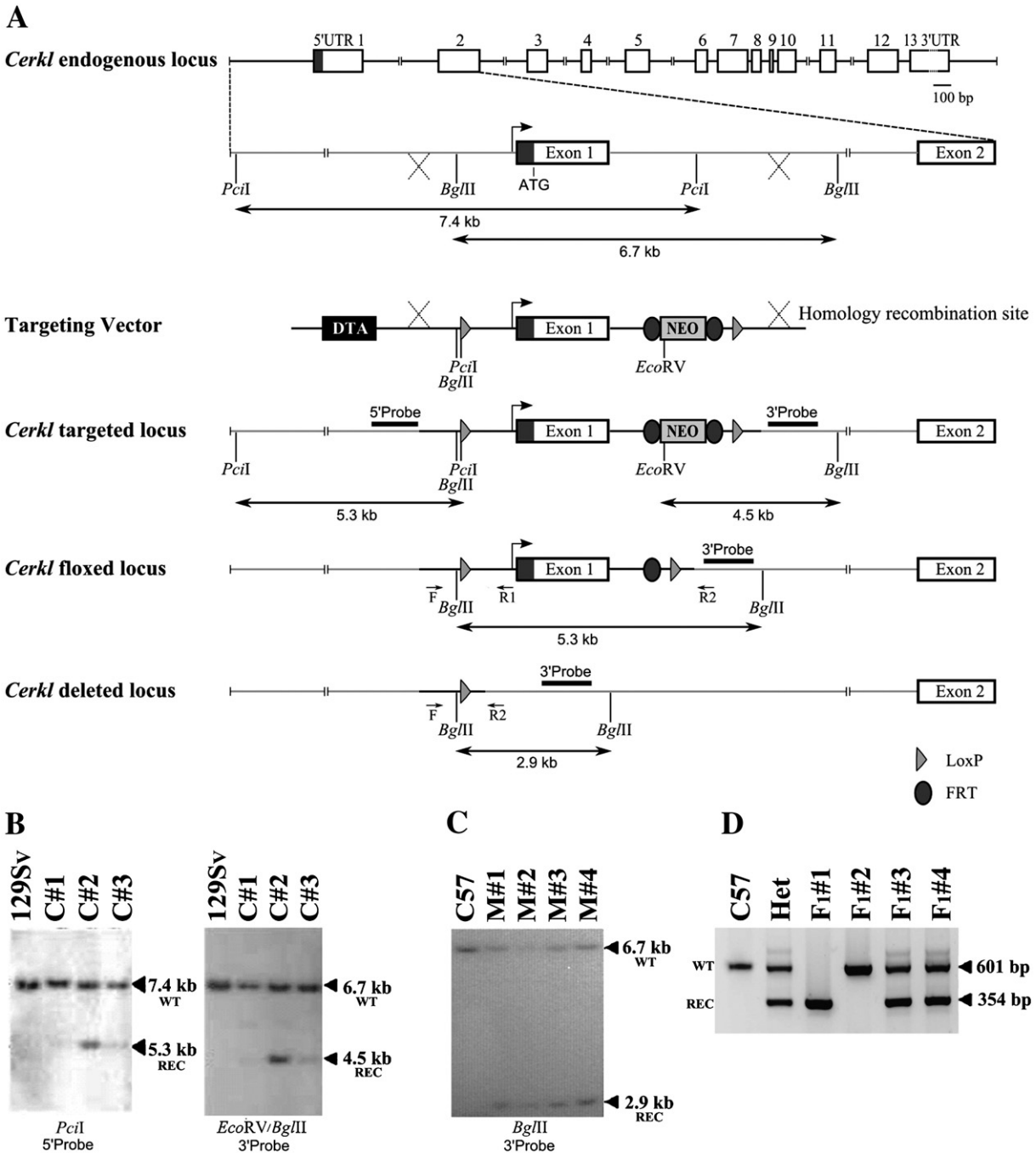

Fig. 1. Targeting of the *Cerkl* locus. (A) Schematic representation of the *Cerkl* locus (drawn to scale), the region of interest encompassing the proximal promoter and first exon, the targeting vector and the targeted, floxed and deleted loci. *Cerkl* exons, Southern blot probes, restriction sites, oligonucleotides for genotyping are depicted. The targeting vector contained the diphteria toxin A (DTA) and neomycin resistance (NEO) genes, the latter flanked by two direct FRT target sites (dark gray ellipses). Two direct loxP sites (light gray triangles) are at the boundaries of the proximal promoter, exon 1 and the NEO cassette. Mice carrying the *Cerkl*^{neo} allele were crossed to a transgenic CMV-Flp recombinase strain to generate the *Cerkl*^{flox} heterozygotes, which were subsequently crossed with a CMV-Cre strain to obtain the *Cerkl*−/− chromosome. (B) Southern blot analysis of targeted ES cells. External probes at 5′ and 3′ were used to verify homologous recombination. Digestion with *Pci*I hybridized with the 5′ probe showed the WT (7.4 kb) and recombinant (5.3 kb) alleles, whereas digestion with *Eco*RV and *Bgl*II with the 3′ probe produced 6.7 kb (WT) and 4.5 kb (recombinant) bands in clones C# 1, 2 and 3. (C) Southern blot of the *Cerkl*+/− mice after the *Bgl*II digestion. The bands observed correspond to WT (6.7 kb) and KO recombinant (2.9 kb) alleles of 4 different heterozygous mice (M# 1, 2, 3 and 5). (D) PCR analysis of the first generation mice obtained after breeding two *Cerkl*+/−. Primers F, R1 and R2 were used in the same PCR reaction. The wt allele produced a band of 601 bp (amplified by F and R1), while the recombinant knockout allele generated a 354 bp band (amplified by F and R2). PCR conditions did not allow the amplification of the band corresponding to the WT allele using the F and R2 primers (2.6 kb).

5 min at 95 °C, then set at 45 cycles in a three-step program: 10 s at 95 °C, 15 s at 62 °C and 10 s at 72 °C. Four replicates were carried out per sample (containing the pooled retinas of at least three different animals), together with their corresponding negative controls. Relative quantification of each gene transcription level was performed using the second-derivative maximum method (LightCycler 480 software, ver. 1.5.0; Roche).

2.5. In situ hybridization and immunohistochemistry on mouse retina cryosections

Eyecups from 2 to 12 month-old WT and KO mice were fixed in 4% paraformaldehyde (PFA) for 2 h at room temperature (RT), washed, and cryoprotected in sucrose at 4 °C (successive incubations at 20% for 30 min, 30% for 30 min and 40% sucrose for 12 h). Eyecups were

Table 1
Sequences of *Cerkl* primers used in the PCR reactions.

Name	Forward primer sequence (5′→3′)	Name	Reverse primer sequence (5′→3′)
Cerkl and Gapdh tissue expression			
*Gapdh*_F	TGAAGGTCGGAGTCAACGGATTTGG	*Gapdh*_R	CATGTAGGCCATGAGGTCCACCAC
mRT_For	CTGACTGTGGTGGTCACTGG	mRT_Rev	GAACCTCTGATGCAGCTTCC
NeuroD1_F	TCAATTTTCCCTTTGTGGAGAC		
UTR_F	TGTAGCCACACTTCCTTCCCA		
3a_F	GTTTTGCTGCGTGGCATCTTC		
3b_F	GACGCATCCAGCCCGAGC		
Riboprobes			
Rho_F	GCCCTTCTCCAACGTCACAG	Rho_R	GCAGCTTCTTGTGCTGTACGG
mRT_For	CTGACTGTGGTGGTCACTGG	mRT_Rev	GAACCTCTGATGCAGCTTCC
Real Time PCR			
β2M_F	GTCTTTCTGGTGCTTGTCTCAC	β2M_R	CGTAGCAGTTCAGTATGTTCGG
Gfap_F	CGCTGGAGGAGGAGATCCA	Gfap_R	ACATCCATCTCCACGTGGACC
Brn3a_F	CCACCCTCCCTGAGCACAAGTA	Brn3a_R	CAGGCTGGCGAAGAGGTTGC
Genotyping			
F	ACACATTAGAAGCCCTGAAGGA	R1	TCTTTGTGCTGTAGCAGTGACC
		R2	TTGCTGTTTAATCCAGTTGTCCT

then embedded in O.C.T (Tissue-Tek, Sakura Finetech, Torrance, CA) and sectioned at −17 °C.

For *in situ* hybridization, 20 μm sections were recovered on poly-lysine covered slides, dried at RT (30 min), rinsed twice with phosphate-buffered saline (PBS) (10 min), treated with 2 μg/ml proteinase K for 15 min at 37 °C, washed twice for 5 min with PBS, and postfixed with 4% PFA. The hybridization was performed as described previously [6] with some modifications: two steps of acetylation with 0.1 M triethanolamine–HCl (pH 8.0) containing 0.25% acetic anhydride and 0.5% were performed (5 min each). The BM Purple AP Substrate (Roche Diagnostics, Indianapolis, IN) reagents were used. Sections were cover-slipped with Fluoprep (Biomérieux, France) and photographed using a Leica DFC Camera connected to a Leica DM IL optic microscope (Leica microsystems, Germany).

For immunohistochemistry, 14 μm sections were recovered on poly-lysine covered slides, dried for 1 h, washed in PBS (3×10 min), and blocked in blocking solution (PBS containing 2% Donkey Serum, 0.2% Triton X-100) at RT (60 min). Incubation with primary antibodies was performed overnight at RT in blocking solution. Sections were rinsed three times in PBS again, followed by incubation with the corresponding secondary antibodies conjugated to either Cy2 or Cy3 (Jackson ImmunoResearch Laboratories, Inc., West Grove, PA) (1:200) at RT (90 min) in blocking solution too. After 3 washes, sections were incubated with DAPI (Sigma-Aldrich, Saint Louis, MO) for 10 min and washed in PBS (3×10 min). Sections were cover-slipped with antifading reagent and photographed with a confocal microscope (LEICA TCS-SP5, Wetzlar, Germany). Primary antibodies and dilutions used were: 1:50 for Goat anti-Brn3a (Santa Cruz Biotechnology, Inc., Santa Cruz, CA); 1:200 for mouse anti-Rhodopsin (BIOTREND Chemikalien GmbH, Cologne, Germany); 1:200 for rabbit anti-PAX6 (Covance, Princeton, NJ) and rabbit anti-blue Opsin, 1:400 for rabbit anti-red/green opsin (Millipore, Billerica, MA); 1:200 for the home-made rabbit anti-CERKL (previously pre-absorbed) and 1:1000 for mouse anti-Calbindin D (Sigma-Aldrich, Sant Louis, MO). GFAP immunostaining was performed as described elsewhere [19] on P60 and P280 WT and KO retina cryosections.

2.6. Protein level analysis

Retinas from P60 and P365 WT and KO mice were homogenized in RIPA buffer (50 mM Tris pH 7.5, 1 mM EDTA, 150 mM NaCl, 0.25% Na-Deoxycholate, 1% NP40 plus protease inhibitors). Thirty micrograms of protein were loaded onto 12.5% acrylamide gels. Western blots were performed as described previously [16]. Primary antibodies were used at the following dilutions: 1:8000 mouse anti-α-tubulin (Sigma-Aldrich, Saint Louis, MO); 1:2500 mouse anti-Rhodopsin and 1:2000 mouse anti-

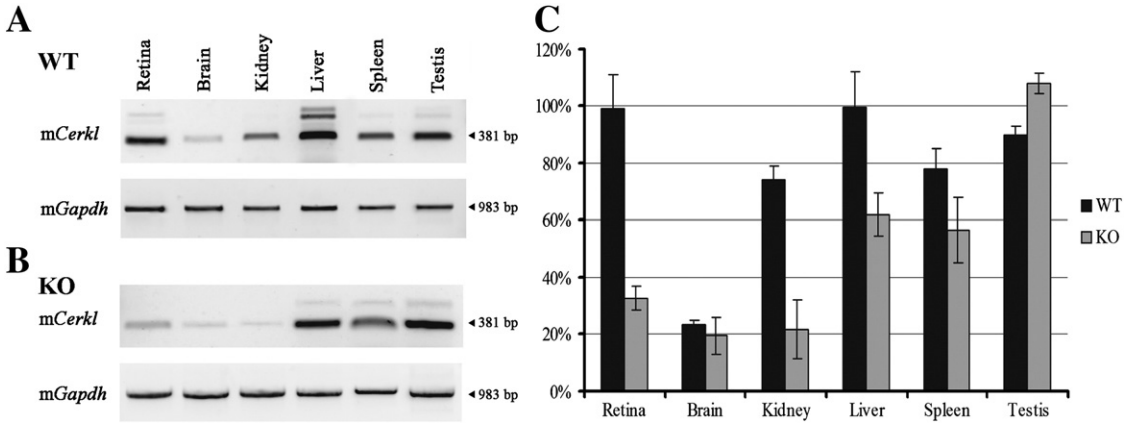

Fig. 2. Semi-quantitative expression analysis of *Cerkl* in wild-type and knockout mice. RT-PCR expression in several tissues of *Cerkl*+/+ (A) and *Cerkl*−/− (B) mice, using primers mRT_F and mRT_R, located in exons 9 and 12, respectively, and contained in all isoforms. Primer sequences are provided in Table 1. The amplicon size is indicated for each case. (C) Semi-quantitative analysis of *Cerkl* expression in *Cerkl*+/+ and *Cerkl*−/− mice. Maximum wild-type *Cerkl* levels were arbitrarily set as 100% (liver). At least three independent replicates were performed. *Gapdh* expression was used for normalization. Significant decreased expression is observed in all KO tissues except brain.

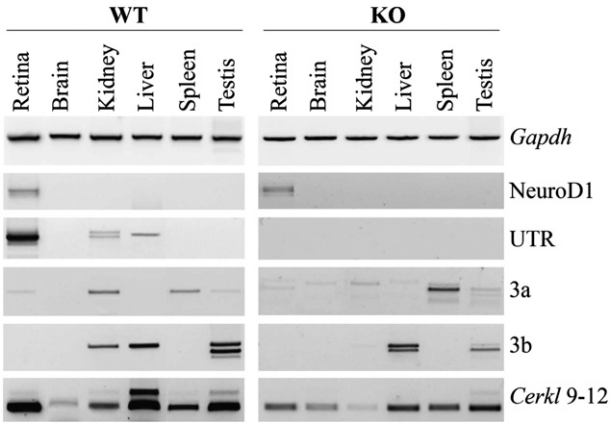

Fig. 3. Remnant *Cerkl* expression in the KO mouse is attained by the use of tissue-specific alternate promoters. RT-PCRs were performed on wild-type and KO murine samples to determine the activity of alternate *Cerkl* promoters in different tissues. Different specific forward primers located at each of the transcription start sites previously identified (*NeuroD1* UTR, *Cerkl* UTR, 3a and 3b) were used in combination with the same reverse oligonucleotide in exon 12. Overall *Cerkl* expression was assessed by amplification of a common region to all isoforms (*Cerkl* 9–12). *Gapdh* was used for normalization. Primer sequences are provided in Table 1.

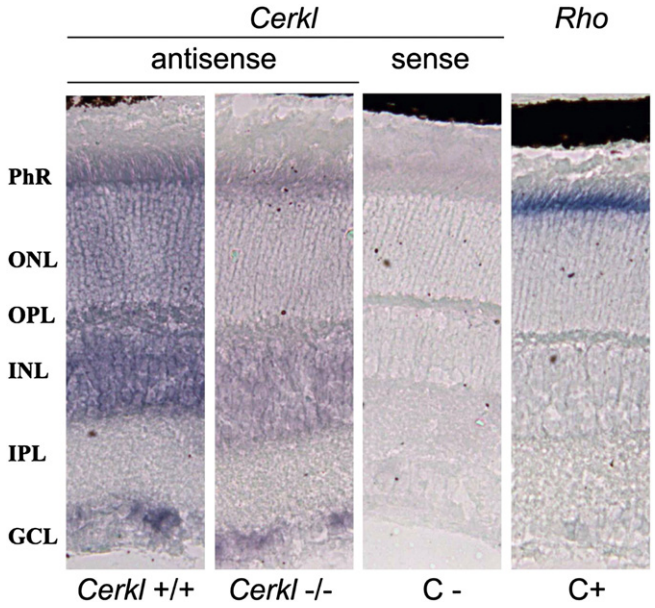

Fig. 4. *Cerkl in situ* hybridization on WT and KO mouse P60 retinas. (A) Representative images (equivalent results in at least three independent replicate animals) of *in situ* hybridizations with the antisense *Cerkl* probe on *Cerkl* +/+ (WT) which labels the GCL, INL and more moderately, the inner photoreceptor segment (dark purple staining). Note that the second panel with the *Cerkl* −/− (KO) retinas shows a much fainter signal in the GCL, INL and the inner photoreceptor segment (light purple staining). Negative control with the sense *Cerkl* probe (C−) and positive control with the antisense *Rhodopsin* probe (C+), which strongly labels the inner photoreceptor segment, are also shown for comparison. PhR— Photoreceptor cell layer; ONL— outer nuclear layer; OPL— outer plexiform layer; INL— inner nuclear layer; IPL— Inner plexiform layer; GCL— ganglion cell layer.

GAPDH (Abcam, Cambridge, UK); 1:2000 mouse anti-PKCα, 1:500 goat anti-RDS, 1:1000 goat anti-Brn3a (Santa Cruz Biotechnology Inc., Santa Cruz, CA); 1:2000 rabbit anti-PAX6 (Covance, Princeton, NJ); 1:2500 mouse anti-GFAP, and 1:2000 rabbit anti-green Opsin and anti-blue Opsin (Millipore, Billerica, MA). Alpha-Tubulin and GAPDH levels were used as normalization controls. Semi-quantification of the bands was carried out using the Quantity One Software (Bio-Rad, Hercules, CA). Statistical significance was analyzed by the Mann–Whitney and t-Student tests.

2.7. TUNEL analysis

Twelve micrometer thick cryostat sections of P60 animals were rinsed in PBS, fixed in ethanol and acetic acid (2:1) for 5 s at −32 °C, then rinsed with PBS and incubated in PBS with 0.2% Triton X-100 and 0.1% Sodium citrate for 15 min. After washing, retinal sections were incubated in TUNEL buffer (30 mM Tris·HCl ph 7.2, 140 mM sodium cacodylate, 1 mM $CoCl_2$, 0.3% Triton-X-100) for 30 min and terminal deoxynucleotidyl transferase (TDT) (800 U/ml) and biotinylated dUTP (1 μM) (Roche Diagnostics, Indianapolis, IN) were added and incubated at 37 °C. The reaction was terminated with SCC×1 buffer and rinsed with PBS. Incubation with goat anti-Brn3a (1:50) (Santa Cruz Biotechnology Inc., Santa Cruz, CA) was performed overnight at room temperature. After washing in PBS, retinal sections were again incubated in a solution containing the secondary antibody anti-goat Cy3 and streptavidin conjugated to Cy2 (Jackson ImmunoResearch Laboratories Inc., West Grove, PA, 1:200 each) for 1 h and 30 min at room temperature. The nuclei were counter-stained with DAPI (Sigma-Aldrich, Saint Louis, MO) and rinsed with PBS. Sections were cover-slipped with antifading reagent and photographed with a confocal microscope (LEICA TCS-SP5, Wetzlar, Germany). A similar protocol was followed for whole-mount preparations.

2.8. Electroretinography

Prior to ERG recording, mice were adapted to the dark overnight. Then, mice were anesthetized under dim red light by i.p. injecting a solution of ketamine (95 mg/kg) and xylazine (5 mg/kg) and maintained on a heated pad at 37 °C. Pupils were dilated by topical application of 1% tropicamide (Alcon, Spain) and flash-induced ERG responses were recorded from both eyes in response to light stimuli produced with a Ganzfeld stimulator. The recording protocol consisted of dark-adaptation for 20 min, after which scotopic ERG, maximum ERG, and dark-adapted oscillatory potentials (OPs) were recorded. After the dark-adapted ERGs, the eyes were light-adapted for 10 min, and the photopic ERG and 30-Hz flicker ERG were recorded. The outcome measures were the response amplitudes and implicit time of each ERG component.

The ERG complied with International Society for Clinical Electrophysiology of Vision (ISCEV) standards [20]. Kruskal–Wallis and Mann–Whitney *U* tests were used to estimate the level of significance for the difference in the ERG parameters among the study groups as appropriate. The ERG signals were amplified and band filtered between 0.3 and 1000 Hz with a Grass amplifier (CP511 AC amplifier, Grass Instruments, Quincy, MA, USA). Electrical signals were digitized at 10 kHz with a Power Laboratory data acquisition board (ADI

Fig. 5. CERKL, Brn3a and Calbindin immunohistochemistry of WT and KO retinas. Fluorescent immunodetection of CERKL, Brn3a (ganglion cell layer marker), Calbindin (amacrine cell marker) and DAPI (nuclear staining) on 14 μm sections from P60 C57BL/6J and *Cerkl* −/− retinas. Photographs were taken in the central retina for comparison. A–D and I–L) WT retinas. E–H and M–P) KO retinas. The CERKL polyclonal antibody (B, F, J and N) reveals a fainter staining in the GCL, INL and the inner photoreceptor segment in the KO vs the WT retinas. The ganglion Brn3a (C and G) and amacrine Calbindin (K and O) cell markers were used. D, H, L, and P are the corresponding merged images. Magnifications of significant parts of Brn3a/CERKL and Calbindin/CERKL merged images are shown at the most right panels. White arrows indicate colocalization of Brn3a and CERKL in the GCL layer (D and H), and Calbindin and CERKL (L and P) in amacrine cells of INL and GCL. PhR— Photoreceptor cell layer; ONL— outer nuclear layer; OPL— outer plexiform layer; INL— inner nuclear layer; IPL— Inner plexiform layer; GCL— ganglion cell layer.

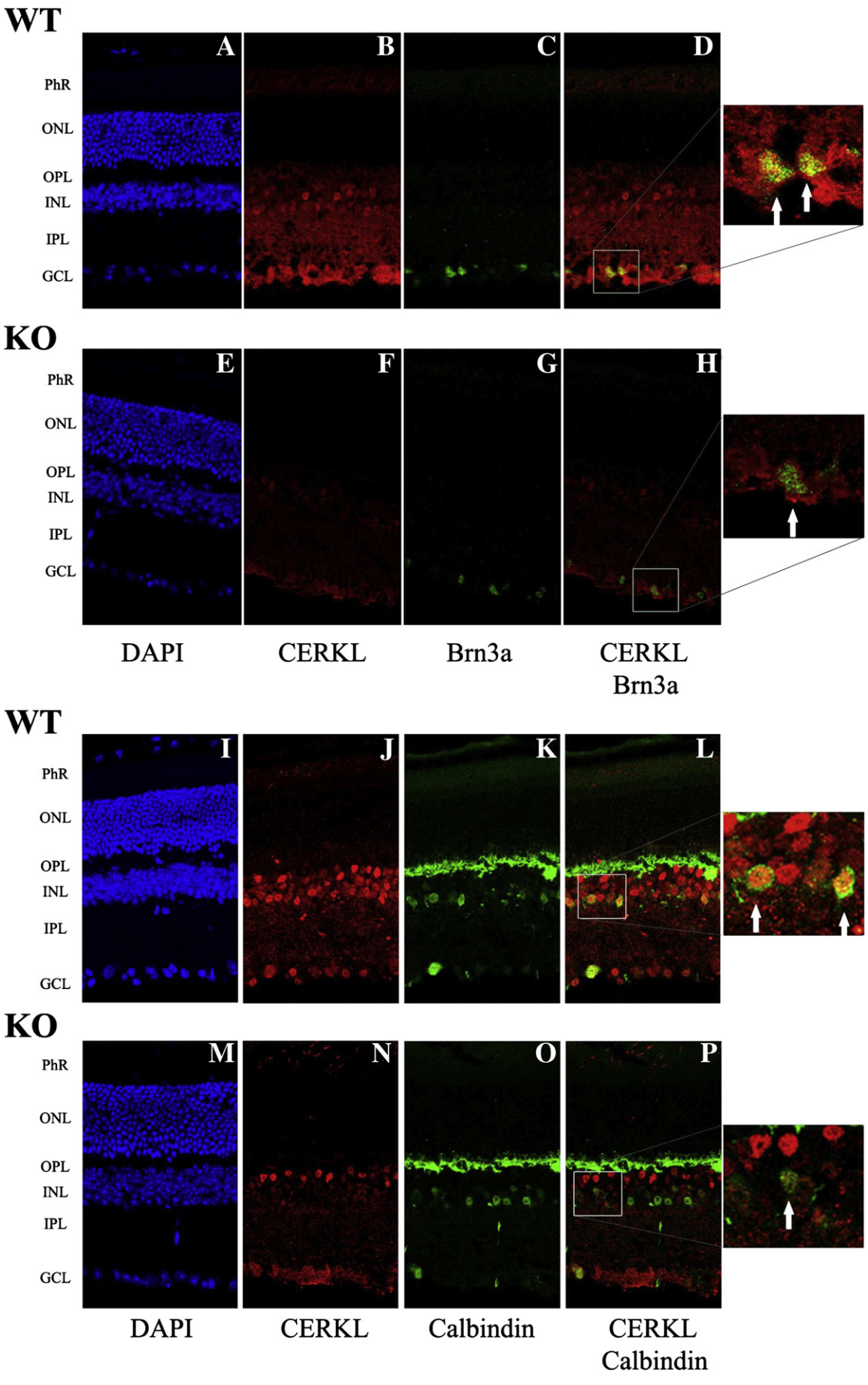
WT
A
B
C
D
PhR
ONL
OPL
INL
IPL
GCL
KO
E
F
G
H
PhR
ONL
OPL
INL
IPL
GCL
DAPI
CERKL
Brn3a
CERKL
Brn3a
WT
I
J
K
L
PhR
ONL
OPL
INL
IPL
GCL
KO
M
N
O
P
PhR
ONL
OPL
INL
IPL
GCL
DAPI
CERKL
Calbindin
CERKL
Calbindin

Instruments, CA, USA). Bipolar recordings were obtained using an Ag: AgCl mouse electrode fixed on a corneal lens (Burian-Allen electrode, Hansen Ophthalmic Lab., IA, USA), a reference electrode located in the mouth, and with a ground electrode located on the tail. The electrode was mounted on a coarse micromanipulator for easy positioning over the mouse eye. Impedance of active and reference electrodes were less than 20 kΩ.

3. Results

3.1. Cerkl deletion of exon 1 and upstream sequences

The gene targeting strategy resulted in the cre-mediated excision of a genomic region of 2.3 kb encompassing the first *Cerkl* exon and the beginning of the first intron, plus 1.2 kb of upstream sequences that stretched the reported promoter (Fig. 1A). Our strategy included a first step of FLP-mediated excision of the neo^R selection gene in the 129/Sv ES cultured cells. All the homologous recombination events performed in the ES cells were assessed by Southern blot analysis (Fig. 1B) using informative restriction enzyme sites and probes specific for the 5′ and 3′ events, depicted in Fig. 1A. Positive clones for the two recombinant events were further confirmed by specific PCR and sequencing, and subsequently used to colonize C57BL/6J blastocysts. Two chimaeric males were obtained and bred to obtain the first heterozygous animals (Fig. 1C), which after successive crosses produced the homozygous null *Cerkl* −/− offspring at the expected mendelian ratio (1:4). Genotyping of tail or ear samples from pups was performed by a single PCR assay (primers indicated in Fig. 1A and Table 1) that allowed the simultaneous amplification of the wild-type and floxed knockout alleles (Fig. 1D) (see Material and methods for details).

3.2. Assessment of Cerkl expression in knockout animals

To assess the abolishment of *Cerkl* expression in the knockout mice, we performed an RT-PCR assay using primers located at the 3′ end of the cDNA, a region common to all the *Cerkl* isoforms reported so far. Contrary to our expectations, the deletion of the reported promoter did not completely abrogate *Cerkl* expression, as a faint band could be observed in retina. These surprising results prompted us to assess the levels of expression in several tissues of the knockout *versus* the wild-type counterparts (Fig. 2A and B).

A semi-quantitative analysis of these results revealed a 65% decrease of *Cerkl* levels in the KO retinas supporting a knockdown model more than a complete knockout (Fig. 2C). Notably, this decrease in *Cerkl* mRNA levels was not homogenous for all tissues, indicating that other promoters, showing tissue specificity, contribute to the final *Cerkl* levels, which is in agreement with recent results showing that at least 3 additional promoters drive *Cerkl* expression in mouse and human [17].

Moreover, a multiple band pattern was observed in some tissues, such as retina, liver, spleen and testis. These bands were excised and sequenced, and correspond to alternatively spliced transcript isoforms, also in agreement with previous data [17].

Once the different *Cerkl* promoters had been identified, we aimed to assess the contribution of each one to the levels of *Cerkl* expression in the different tissues of the KO mice compared to the wild-type controls. Indeed, as expected by the design of the targeting and the genotyping of the KO mice, no transcripts from the reported *Cerkl* promoter were observed in any tissue (Fig. 3, UTR). Concerning the expression of *Cerkl* in the KO retina, residual transcription from the upstream *NeuroD1* gene and internal *Cerkl* 3a promoters can be detected at similar levels than the WT retinas, accounting for the 30–35% of the total *Cerkl* transcripts (Figs. 2 and 3). The major isoforms in *Cerkl* −/− retinas are two transcripts starting at *NeuroD1* and one from the internal 3a promoter, indicated with a symbol (#) in the Supplementary Fig.1.

Although no compensatory transcriptional activation from the alternative promoters in the KO tissues was detected, moderate transcriptional differences were observed, such as decreased expression in kidney and testis from 3a and 3b, increased expression in spleen, and specific isoform patterns in liver and testis (Fig. 3).

3.3. Morphological analysis of the KO retina

Retinal sections of KO mouse obtained at 2, 4 and 12 months stained with hematoxylin/eosin did not show any gross morphological differences neither in the cell layer organization, nuclei density or photoreceptor outer segment length, when compared to WT animals of the same age (Supplementary Fig. 2A). Nuclear counts after staining with DAPI visualized in the confocal microscopy did not reveal any significant difference in the density and distribution through all the layers at four different retina eccentricities (Supplementary Fig. 2B).

The localization of *Cerkl* expression products was then addressed to assess possible differences in intensity/distribution throughout the retinal cell layers. To this aim, *in situ* mRNA hybridization was performed with a riboprobe against the shared RNA region of all isoforms (stretching exons 8 to 12), using *Rhodopsin* antisense and *Cerkl* sense riboprobes as positive and negative controls, respectively. In agreement with previous findings, WT endogenous *Cerkl* is mainly detected in the GCL, and moderate expression at the inner segment of photoreceptors (PhR) and the INL (Fig. 4). As expected, *Cerkl* mRNA levels is decreased in the retina of the KO mouse, as shown by a considerable decrease in hybridization intensity compared to the WT controls, treated and stained under the same conditions and time (Fig. 4). Notably, the more prominent decrease is observed in the GCL, followed by the INL and much less in the PhR, indicating that there is not a homogeneous decrease in *Cerkl* expression.

3.4. Immunolocalization of CERKL

Immunodetection of adult mouse retinas with an in-house anti-CERKL polyclonal antibody (raised against a peptide encoded in mouse *Cerkl* exon 2) indicated that CERKL localized in the GCL, INL, and PhR (Fig. 5). In photoreceptors and INL cells, CERKL was shown to be exclusively located in the cytoplasm and no nuclear staining was observed in these cell types, as it has been described before [21]. A fainter staining in the GCL, INL and the photoreceptor layer with our CERKL polyclonal antibody was observed in the KO retinas. Immunohistochemical stainings using antibodies against Brn3a and Calbindin, specific retinal cell markers, showed cytoplasmic colocalization of CERKL with a population of ganglion and amacrine cells but no apparent change in the number and/or distribution of stained cells (Fig. 5). A similar analysis with the retinal cell marker PAX6 did not show any expression pattern alteration either (Supplementary Fig. 3). *Cerkl* −/− mouse retinas did not show any sign of rod and cone degeneration after rhodopsin/opsin immunostaining, even at 12 months of age (data not shown). Besides, the photoreceptor outer segment length (average ~ 22 μm), diameter and density were preserved, consistent with neither photoreceptor degeneration nor apoptosis (data not shown).

Given that no clear signals of apoptosis were detected in the *Cerkl* −/− retinas, and that previous results from our group showed that overexpression of CERKL protected cells against oxidative stress injuries [16], we searched for other signals of retinal stress. Glial fibrillary acid protein (GFAP) expression is usually restricted to Müller cell endfeet in the inner limiter membrane [19], but its expression is increased and may extend to other retinal cell layers upon aging and retinal stress. Immunohistochemistry analysis on P60 and P280 WT and KO retinas was performed. Differences in GFAP distribution and expression between WT and KO retinas were very slight, although the expected increase of GFAP with age was clearly detectable in both WT and KO retinas (Supplementary Fig. 4).

3.5. Retinal protein marker expression in KO retinas

To assess the effects of the diminished *Cerkl* expression on several retinal markers, indicative of structural/functional alterations in retinal cell layers, we performed a semi-quantitative immunodetection on Western blots in P60 WT and KO retinal lysates. Markers of the functional status of: cones and rods (green opsin, blue opsin and rhodopsin), ganglion (Brn3a), amacrine/ganglion (PAX6) and bipolar (α-PKC) cells, and retinal stress (GFAP) were immunodetected and analyzed (Fig. 6A). Notably, a statistically significant decrease of Brn3a, but not of PAX6 was detected (Fig. 6B), which indicates a perturbed structural/functional status of the ganglion cells, rather than amacrine cells. Moreover, the GFAP expression is clearly increased, revealing higher levels of retinal stress in the *Cerkl* −/− animals. These results prompted us to analyze the evolution of these altered expression levels with age (Fig. 6C). In one-year (P365) aged animals, the decrease of Brn3a expression remains consistent and at comparable levels than those of P60 mice. Concerning GFAP, relative differences between WT and KO retinas are

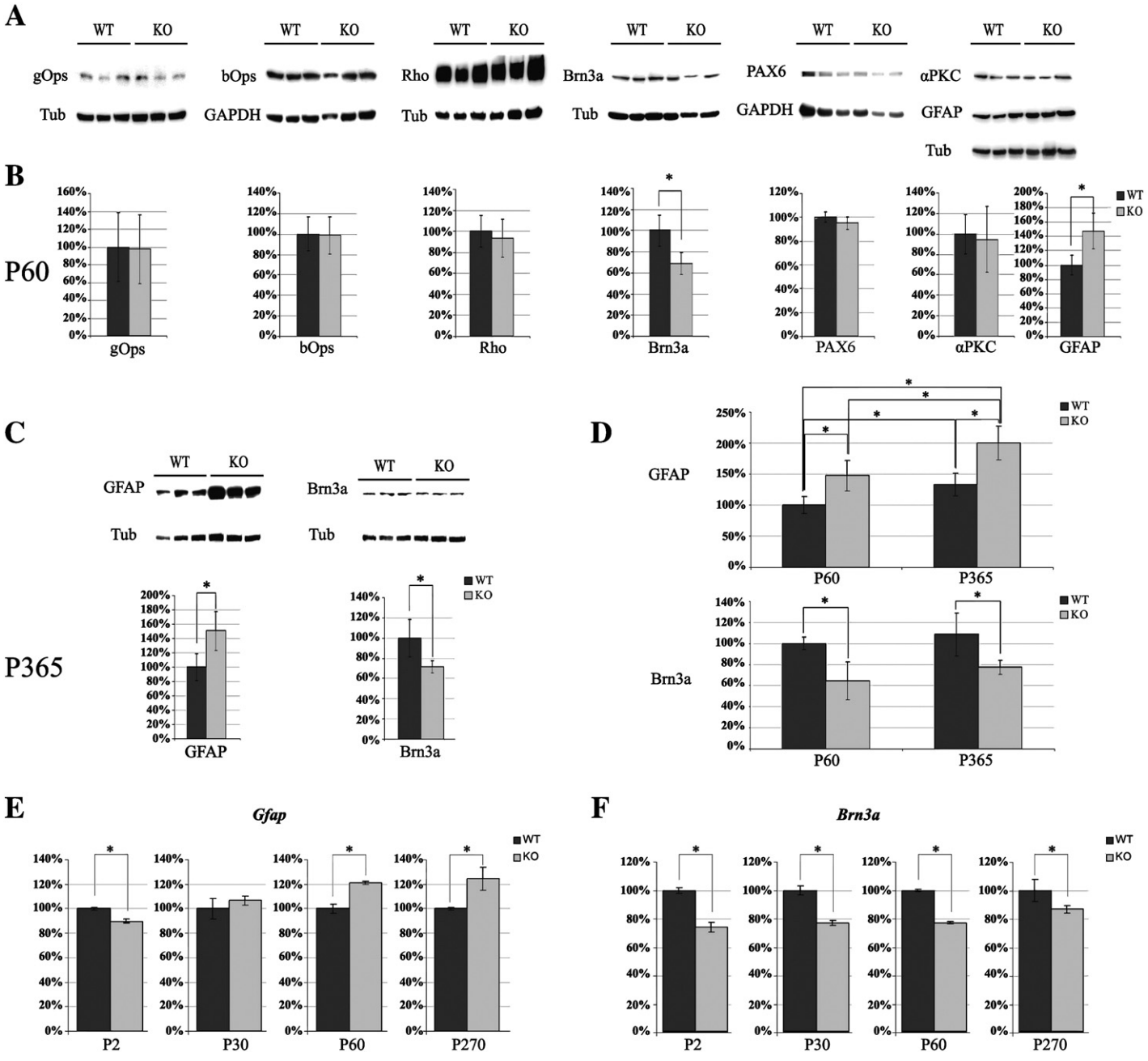

Fig. 6. Semi-quantification by Western blot of retinal proteins in WT and KO mice. (A) Thirty micrograms of P60 protein lysates of WT and KO mice retinas was immunodetected with antibodies against the green and blue opsins, rhodopsin, GFAP, Brn3a, PAX6 and α-PKC proteins. Tubulin and GAPDH were used as controls for normalization. (B) Semi-quantified proteins are depicted in the histograms. For each age, WT levels were considered as 100%. Only GFAP and Brn3a showed significant differences (* $p<0.05$, t-Student). (C) Immunodetection and quantification of GFAP and Brn3a markers in lysates of P365 WT and KO mice retinas. For each age, WT levels were considered as 100%. (D) Expression of GFAP and Brn3a at P60 (100%) and P365 between WT and KO. GFAP levels were increased in aged animals, although the ratio WT/KO appears to be maintained (45–50%) (* $p<0.05$, t-Student). No statistically significant differences were observed in Brn3a levels between P60 and P365 animals. (E and F) Quantitative RT-PCR assessment of *Gfap* (E) and *Brn3a* (F) transcriptional levels in WT and KO retinas at P2, P30, P60 and P270. *β-2-microglobulin* levels were used for normalization between samples. For each age, WT levels were considered as 100%. Each value contained the mRNA of at least three different animals, and at least four different replicates were analyzed for each point (* $p<0.05$, t-Student).

also maintained at the same level (around 50% increase), and indeed, GFAP levels increase proportionally in the two groups due to aging (Fig. 6D).

To further support the decrease of Brn3a and increase of GFAP expression in WT and KO retinas, we assessed the levels of transcription of their corresponding genes by quantitative RT-PCR, including *β-2-microglobulin* as a normalization control. In addition, to test whether these differences in expression were constitutive or progressive during retinal development until maturation, several earlier time points (postnatal days 2 and 30) were added to the analysis. The transcriptional analyses reinforced the data gathered by protein levels immunodetection. Thus, KO retinas showed a progressive increase of *Gfap* expression (compared to WT retinas), indicative of more vulnerability to retinal stress with age (Fig. 6E). In contrast, the diminished Brn3a transcription levels appear to be a constitutive trait of the KO retinas, as it is already evident as early as in P2 animals, and the difference with the WT retinas is maintained with age (Fig. 6F).

The fact that no differences are observed in the other protein markers analyzed highlights that the effect on Brn3a and GFAP expression is specific and reflects the altered status of the KO retinas.

3.6. TUNEL analysis

To assess whether this altered status of the *Cerkl* −/− retinas was also reflected in an increase of cell death, the levels of apoptosis were analyzed by TUNEL staining on whole-mount and retinal sections (Fig. 7A and B, respectively). Twelve retinal regions on the whole-mounts were selected for systematic counting and analysis for each eye from a total of three animals in each experimental group. Increased levels of apoptotic cells (more than two-fold) were clearly observed in the KO vs WT retinas (Fig. 7A), and this increase was statistically significant (Fig. 7C, $p<0.01$). In order to elucidate whether the observed decrease in Brn3a expression correlated with specific death of the Brn3a subset of ganglion cells, co-immunostaining in retina sections was performed (Fig. 7B). Our results show that apoptosis affects some but is not restricted to Brn3a positive ganglion cells, indicating that the *Cerkl* −/− retinal perturbation involves different cell types.

3.7. Electroretinographic characterization of the KO retinas

The ERG experiments were performed in 10 C57BL/6J and 12 *Cerkl*−/− mice, measured four times at 2–3 months of age and at 3 month intervals until the animals reached 12 months. The ERG did not show significant differences between *Cerkl* −/− and WT mice through time in response amplitudes and implicit times neither for scotopic ERG, maximum ERG a- and b-waves, nor for photopic single-flash a-wave and 30-Hz flicker ERG. Interestingly, a significant decrease in the amplitudes of oscillatory potentials (OPs) in the *Cerkl* −/− mice was observed (Fig. 8). Although the frequency analysis showed no significant differences in the power spectral density at different frequency bands (0–60, 60–120 and 120–180 Hz) (data not shown), most OP components (OP2–OP4) were significantly reduced in amplitude and increased in implicit time in the KO compared with WT animals ($P<0.05$, Mann–Whitney test). These changes were first seen at P60 and remained consistent at P180 and up to P360, but showed no progression. Most interestingly, the OP/a and OP/b ratios in the KO animals did differ significantly compared to amplitudes measured in age-matched wild-type C57BL/6J mice ($P<0.05$, Mann–Whitney test). Together with the same b/a ratio values in both strains, it could be suggested that the neuronal circuitries of the inner retina are moderately affected in this *Cerkl* −/− model.

4. Discussion

Mutations in human *CERKL* cause progressive retinal degeneration leading to CRD or RP [1–8]. Despite a close structural similarity with CERK, all the attempts to characterize its putative lipid kinase enzymatic activity have failed so far [14–16]. Taking into consideration: 1) the high transcriptional complexity of *CERKL*; 2) the large range of protein isoforms, which display different domains; 3) the wide retinal expression pattern of *Cerkl,* not exclusive of photoreceptors; and 4) the highly dynamic nuclear–cytoplasmic protein localization, all together underscore the challenge behind the dissection of the CERKL functional role and contribution to retinal dystrophies.

Following the conventional approach for functional analysis of human genes associated to hereditary diseases, we aimed to generate a novel knockout mouse model, *Cerkl*−/−. Other authors had previously attempted to emulate the most common mutation allele (R257X) by deleting exon 5, but this model did not show any retinal phenotype nor alterations in the levels of ceramide/C1P in the retina [18]. The lack of ocular phenotype could be explained by the fact that this exon is alternatively spliced and thus, the remaining isoforms could perform some of the *Cerkl* roles [17]. Therefore, we aimed to construct a total knockout model by a loxP/cre-based deletion of the *Cerkl* first exon plus 1.2 kb upstream region that encompassed the proximal promoter and transcriptional initiation site.

Although the gene targeting was successful, *Cerkl* expression could not be completely abrogated. Unfortunately, some basal transcription (around 30–35%) was driven by previously unreported alternative promoters, among them that of *NeuroD1* gene, which accounts for most of the remaining *Cerkl* expression in the KO mice retina. This promoter is located upstream the *Cerkl* gene, transcribes the same DNA strand, and is highly active in the Central Nervous System (CNS). Sequencing revealed that these transcripts started at the 5′ UTR first exon of the *NeuroD1* gene, followed by a cryptic intergenic 173-bp exon joined to *Cerkl* exon 2. The fact that this cryptic exon contains several methionines, one of them in frame, supports that some CERKL could be present in the KO retina. In this respect, evidences that other CERKL initiating methionines could be recognized *in vivo* in other isoforms have already been gathered in human [17]. Indeed, the *Cerkl* isoforms arising from this promoter could explain the mild retinal phenotype, befitting more a knockdown than a knockout model.

Overall, our results indicate that in the retina the alternative promoters (*NeuroD1* and *Cerkl* 3a and 3b) do not show transcriptional compensatory activity in the KO mice (Fig. 3). However, small differences in the *Cerkl* expression pattern could be detected in other tissues: a slight increase could be detected in testis, and new isoforms were apparent in kidney, liver, and testis. Either the deletion of upstream *Cerkl* sequences or changes in the relative position of the proximal regulatory elements in the *floxed* allele may account for these differences. Further work is required to assess the validity of these hypotheses.

In our electroretinographic studies, ERG amplitudes and latencies of scotopic a-waves and b-waves, and photopic b-waves in the *Cerkl* −/− were not significantly decreased compared to age-matched WT mice, which indicated that the basic pathways of phototransduction and signal transmission in the outer retina were unaffected. However, the consistently observed differences in the OPs (high frequency (90–160 Hz), low amplitude wavelets on the rising edge of the electroretinogram (ERG) b-wave) pointed to functional alterations in the inner plexiform layer (IPL), even though the morphology was preserved.

Multiple cell types in the inner retina – in particular at the IPL [22] – could contribute to OPs, but amacrine and/or ganglion cells are the largest contributors [23,24]. In this context, early and late components of OPs appear to be modulated independently [25,26], and may reflect the functional contribution of these two distinct cell groups. In the KO animals, late OP components (OP3) were significantly reduced in amplitude and increased in implicit time (Fig. 7). Notably, it

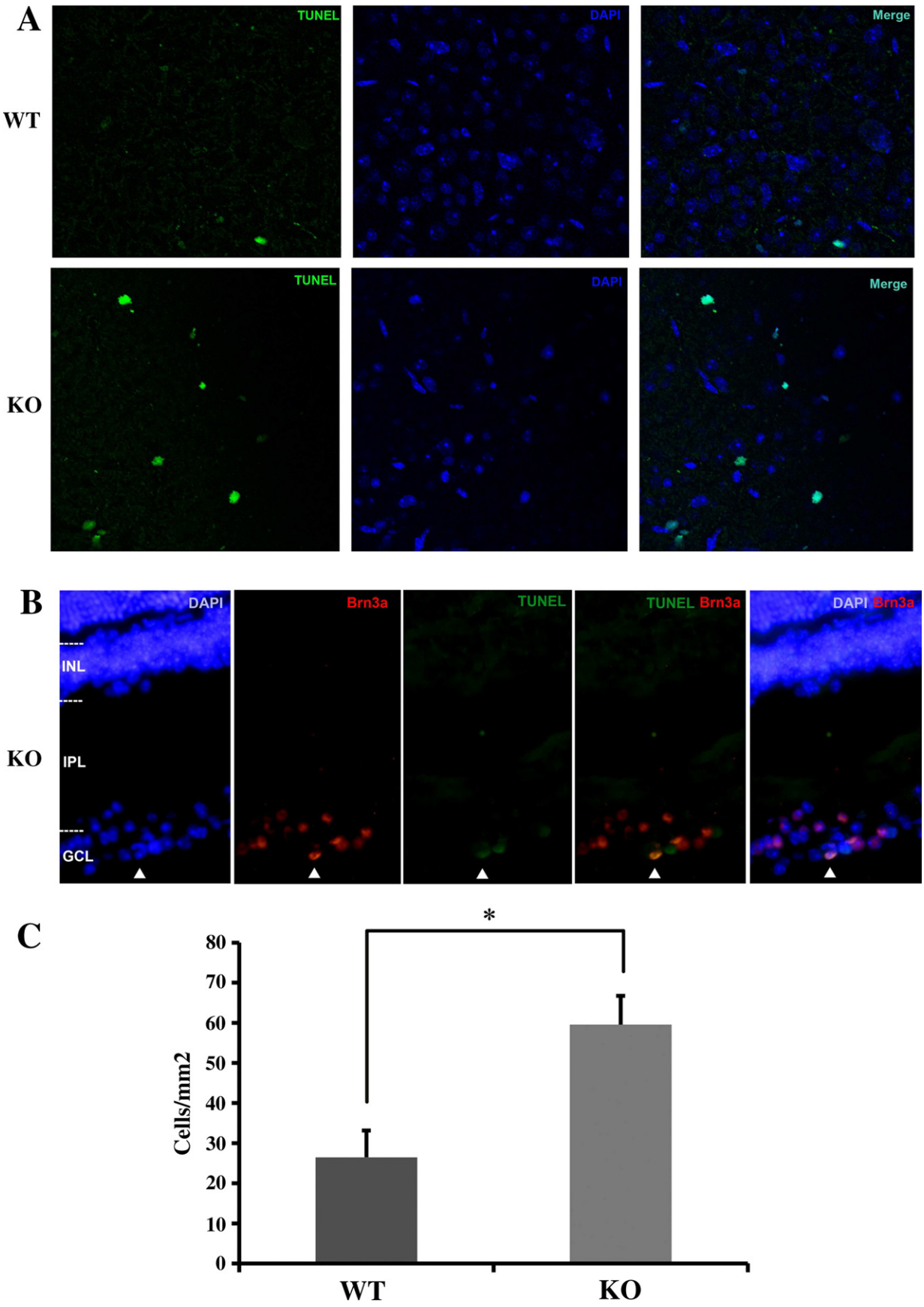

Fig. 7. Increased apoptosis in the P60 *Cerkl* −/− retinas. (A) Nasal region images of TUNEL analyses performed on whole-mount retinas of the *Cerkl* −/− (KO) and wild type (WT) animals, focused on the GCL. (B) Double staining of Brn3a and TUNEL positive cells in sections of the *Cerkl* −/− (KO) retinas. Arrowheads indicate the colocalization of the different labels in a ganglion cell. Note that neither all TUNEL positive cells are Brn3a positive, nor apoptosis is restricted to Brn3a cells. (C) TUNEL positive cell counts for WT and KO retinas (twelve different regions per retina and three different animals per group). Statistically significant differences (* $p<0.01$, t-Student test) were observed.

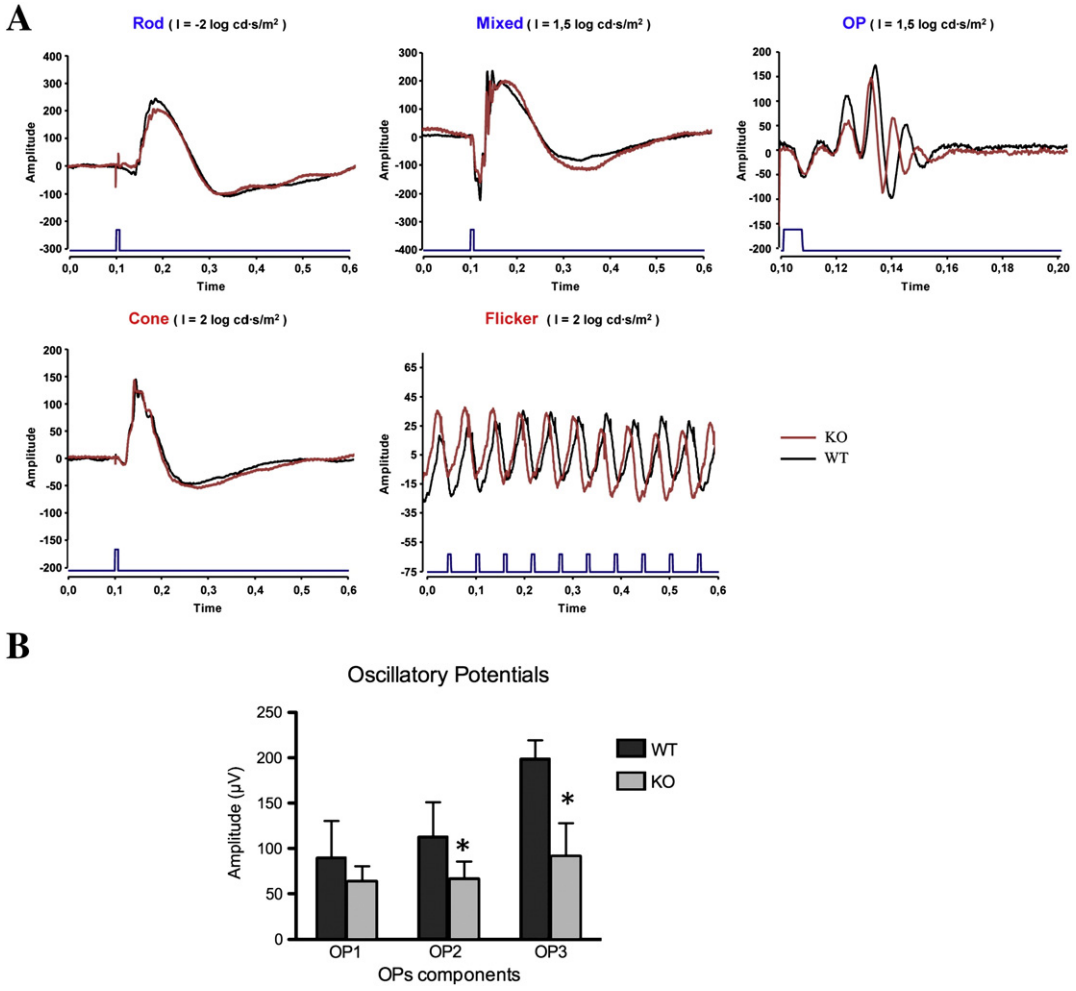

Fig. 8. Electroretinographic responses from control C57BL/6J (black) and *Cerkl*−/− mice (red) at P120. (A) Superimposed response waveforms of various ERG components from one control (black traces) and one *Cerkl* −/− mouse (red traces): Rod responses to light flashes of −2.09 log cd s m^{-2} and mixed responses (rod and cone) to light flashes of 1.57 log cd s m^{-2} were recorded under dark adaptation. Cone responses (photopic ERG, oscillatory potentials and 30 Hz) Flicker) were recorded under light adaptation to light flashes of 1.57 log cd s m^{-2}. Horizontal calibration: 100 ms; vertical calibration: 50 μV. (B) Histogram representation of the power spectral density (PSD) (mean and SD) of Oscillatory Potentials measured in C57BL/6J *Cerkl*+/+ (n = 8) and *Cerkl*−/− animals (n = 8) (* $p<0.05$, Mann–Whitney test).

has been shown that deletion of Brn3a in mouse dramatically alters the dendritic stratification at the IPL, with very moderate ganglion cell loss [27]. Given that dentritic arborization correlates with physiological responses, the decrease of Brn3a (apparently constitutive in our model) could be the cause of the observed OP alterations. Therefore, our data favors alteration of ganglion over amacrine cells on the grounds of reduced OP waveforms, decreased expression of Brn3a and unperturbed levels of PAX6 and calbindin. We cannot rule out that other retinal cell types might be functionally disturbed, as reflected by the increased apoptosis and higher expression of the retinal stress marker GFAP.

Why the mouse *Cerkl* −/− retinal phenotype differs from that of human patients? In order to answer this question, it may be relevant to compare the gathered data. First, adult mouse retinas mainly express *Cerkl* in the GCL ([6] and this work) and the *Cerkl* −/− retina alterations point to ganglion cell affectation; in contrast, the analysis of the human *CERKL* patients has revealed that GCL thickness and altered nerve fiber layer (NFL) only appears at late disease stages [2,7]. Second, a thickening of the superficial hyperreflective layer normally ascribed to the retinal nerve fiber layer (NFL) has been observed in patients, most probably due to increased glial processes [7]; in contrast, the increased gliosis (higher GFAP immunoreactivity) observed in the KO mice retinas did not relate to NFL hyperreflectivity. Third, concerning photoreceptor functional integrity, while full-field ERGs with negative waveforms (greater b- than a-wave amplitude reduction) are a feature of severely affected *CERKL* patients [7], this alteration could not be observed in our KO model (in agreement with preservation of rods and cones at the analyzed times), and only OP components appear reduced. All these observations could be reconciled if human and mouse retinas respond differently to the same genetic defect and/or to stress insults. Other explanations for this mild ocular phenotype in our *Cerkl* −/− mouse may rely on *Cerkl* being partially redundant in mouse – so that other genes compensate for its deletion –, or on species-specific expression patterns at the retinal level — so that the phenotype caused by mutations in mouse does not have to abide to the severity observed in humans. Indeed, the same type of arguments has also been proposed for knockout models of other RD-causative genes with no phenotypic visual alterations, such as the *Rdh12*, *Gcap2* and *Gcap1/2* KO mice [28–31].

In summary, our *Cerkl* −/− model shows consistent perturbation of the GCL, as reflected by altered OP waveforms and lower levels of Brn3a, a POU-homeobox transcription factor involved in synaptogenesis and axonogenesis [27,32,33]. These results together with the consistent increased retinal stress and apoptosis signals observed in *Cerkl* −/− retinas further expand the role of *Cerkl* to the homeostasis, preservation and physiology of retinal neurons.

Acknowledgments

We would like to acknowledge the technical contribution of Laura Ramírez. A.G and M.R were in receipt of the fellowships FPI BES-2007-15414 and FPU AP2007-00805.

Grant information: this study was supported by grants BFU2006-04562 (Ministerio de Educación y Ciencia), SAF2009-08079 (Ministerio de Ciencia e Innovación), 2009SGR-1427 (Generalitat de Catalunya), CIBERER (U718), Retina-Asturias and ONCE to R.G.-D; SAF2007-66175 and SAF2010-21879 (Ministerio de Educación y Ciencia); RD07/0062/0008 (Instituto de Salud Carlos III) to P. de la V., FISS PI11/00533 (Instituto de Salud Carlos III) to R.B. and BFU2010-15656 (Ministerio de Educación y Ciencia) to G. M.

Appendix A. Supplementary data

Supplementary data to this article can be found online at http://dx.doi.org/10.1016/j.bbadis.2012.04.004.

References

[1] M. Ali, V.L. Ramprasad, N. Soumittra, M.D. Mohamed, H. Jafri, Y. Rashid, M. Danciger, M. McKibbin, G. Kumaramanickavel, C.F. Inglehearn, A missense mutation in the nuclear localization signal sequence of CERKL (p.R106S) causes autosomal recessive retinal degeneration, Mol. Vis. 14 (2008) 1960–1964.
[2] N. Auslender, D. Sharon, A.H. Abbasi, H.J. Garzozi, E. Banin, T. Ben-Yosef, A common founder mutation of CERKL underlies autosomal recessive retinal degeneration with early macular involvement among Yemenite Jews, Invest. Ophthalmol. Vis. Sci. 48 (2007) 5431–5438.
[3] A. Avila-Fernandez, R. Riveiro-Alvarez, E. Vallespin, R. Wilke, I. Tapias, D. Cantalapiedra, J. Aguirre-Lamban, A. Gimenez, M.J. Trujillo-Tiebas, C. Ayuso, CERKL mutations and associated phenotypes in seven Spanish families with autosomal recessive retinitis pigmentosa, Invest. Ophthalmol. Vis. Sci. 49 (2008) 2709–2713.
[4] E. Pomares, G. Marfany, M.J. Brion, A. Carracedo, R. Gonzalez-Duarte, Novel high-throughput SNP genotyping cosegregation analysis for genetic diagnosis of autosomal recessive retinitis pigmentosa and Leber congenital amaurosis, Hum. Mutat. 28 (2007) 511–516.
[5] Z. Tang, Z. Wang, Z. Wang, T. Ke, Q.K. Wang, M. Liu, Novel compound heterozygous mutations in CERKL cause autosomal recessive retinitis pigmentosa in a nonconsanguineous Chinese family, Arch. Ophthalmol. 127 (2009) 1077–1078.
[6] M. Tuson, G. Marfany, R. Gonzalez-Duarte, Mutation of CERKL, a novel human ceramide kinase gene, causes autosomal recessive retinitis pigmentosa (RP26), Am. J. Hum. Genet. 74 (2004) 128–138.
[7] T.S. Aleman, N. Soumittra, A.V. Cideciyan, A.M. Sumaroka, V.L. Ramprasad, W. Herrera, E.A. Windsor, S.B. Schwartz, R.C. Russell, A.J. Roman, C.F. Inglehearn, G. Kumaramanickavel, E.M. Stone, G.A. Fishman, S.G. Jacobson, CERKL mutations cause an autosomal recessive cone-rod dystrophy with inner retinopathy, Invest. Ophthalmol. Vis. Sci. 50 (2009) 5944–5954.
[8] K.W. Littink, R.K. Koenekoop, L.I. van den Born, R.W. Collin, L. Moruz, J.A. Veltman, S. Roosing, M.N. Zonneveld, A. Omar, M. Darvish, I. Lopez, H.Y. Kroes, M.M. van Genderen, C.B. Hoyng, K. Rohrschneider, M.J. van Schooneveld, F.P. Cremers, A.I. den Hollander, Homozygosity mapping in patients with cone-rod dystrophy: novel mutations and clinical characterizations, Invest. Ophthalmol. Vis. Sci. 51 (2010) 5943–5951.
[9] M. Sugiura, K. Kono, H. Liu, T. Shimizugawa, H. Minekura, S. Spiegel, T. Kohama, Ceramide kinase, a novel lipid kinase. Molecular cloning and functional characterization, J. Biol. Chem. 277 (2002) 23294–23300.
[10] S.M. Bajjalieh, T.F. Martin, E. Floor, Synaptic vesicle ceramide kinase. A calcium-stimulated lipid kinase that co-purifies with brain synaptic vesicles, J. Biol. Chem. 264 (1989) 14354–14360.
[11] Y.A. Hannun, L.M. Obeid, Principles of bioactive lipid signalling: lessons from sphingolipids, Nat. Rev. Mol. Cell Biol. 9 (2008) 139–150.
[12] G.E. Miranda, C.E. Abrahan, L.E. Politi, N.P. Rotstein, Sphingosine-1-phosphate is a key regulator of proliferation and differentiation in retina photoreceptors, Invest. Ophthalmol. Vis. Sci. 50 (2009) 4416–4428.
[13] O.L. German, G.E. Miranda, C.E. Abrahan, N.P. Rotstein, Ceramide is a mediator of apoptosis in retina photoreceptors, Invest. Ophthalmol. Vis. Sci. 47 (2006) 1658–1668.
[14] F. Bornancin, D. Mechtcheriakova, S. Stora, C. Graf, A. Wlachos, P. Devay, N. Urtz, T. Baumruker, A. Billich, Characterization of a ceramide kinase-like protein, Biochim. Biophys. Acta 1687 (2005) 31–43.
[15] Y. Inagaki, S. Mitsutake, Y. Igarashi, Identification of a nuclear localization signal in the retinitis pigmentosa-mutated RP26 protein, ceramide kinase-like protein, Biochem. Biophys. Res. Commun. 343 (2006) 982–987.
[16] M. Tuson, A. Garanto, R. Gonzalez-Duarte, G. Marfany, Overexpression of CERKL, a gene responsible for retinitis pigmentosa in humans, protects cells from apoptosis induced by oxidative stress, Mol. Vis. 15 (2009) 168–180.
[17] A. Garanto, M. Riera, E. Pomares, J. Permanyer, M. de Castro-Miro, F. Sava, J.F. Abril, G. Marfany, R. Gonzalez-Duarte, High transcriptional complexity of the retinitis pigmentosa CERKL gene in human and mouse, Invest. Ophthalmol. Vis. Sci. 52 (2011) 5202–5214.
[18] C. Graf, S. Niwa, M. Muller, B. Kinzel, F. Bornancin, Wild-type levels of ceramide and ceramide-1-phosphate in the retina of ceramide kinase-like-deficient mice, Biochem. Biophys. Res. Commun. 373 (2008) 159–163.
[19] D. Chakraborty, S.M. Conley, M.W. Stuck, M.I. Naash, Differences in RDS trafficking, assembly and function in cones versus rods: insights from studies of C150S-RDS, Hum. Mol. Genet. 19 (2010) 4799–4812.
[20] M.F. Marmor, G.E. Holder, M.W. Seeliger, S. Yamamoto, Standard for clinical electroretinography (2004 update), Doc. Ophthalmol. 108 (2004) 107–114.
[21] S. Vekslin, T. Ben-Yosef, Spatiotemporal expression pattern of ceramide kinase-like in the mouse retina, Mol. Vis. 16 (2011) 2539–2549.
[22] L. Wachtmeister, Oscillatory potentials in the retina: what do they reveal, Prog. Retin. Eye Res. 17 (1998) 485–521.
[23] B.V. Bui, B. Fortune, Ganglion cell contributions to the rat full-field electroretinogram, J. Physiol. 555 (2004) 153–173.
[24] B. Fortune, B.V. Bui, J.C. Morrison, E.C. Johnson, J. Dong, W.O. Cepurna, L. Jia, S. Barber, G.A. Cioffi, Selective ganglion cell functional loss in rats with experimental glaucoma, Invest. Ophthalmol. Vis. Sci. 45 (2004) 1854–1862.
[25] C.J. Dong, P. Agey, W.A. Hare, Origins of the electroretinogram oscillatory potentials in the rabbit retina, Vis. Neurosci. 21 (2004) 533–543.
[26] P. Lachapelle, J.M. Little, R.C. Polomeno, The photopic electroretinogram in congenital stationary night blindness with myopia, Invest. Ophthalmol. Vis. Sci. 24 (1983) 442–450.
[27] T.C. Badea, H. Cahill, J. Ecker, S. Hattar, J. Nathans, Distinct roles of transcription factors brn3a and brn3b in controlling the development, morphology, and function of retinal ganglion cells, Neuron 61 (2009) 852–864.
[28] I. Kurth, D.A. Thompson, K. Ruther, K.L. Feathers, J.D. Chrispell, J. Schroth, C.L. McHenry, M. Schweizer, S. Skosyrski, A. Gal, C.A. Hubner, Targeted disruption of the murine retinal dehydrogenase gene Rdh12 does not limit visual cycle function, Mol. Cell. Biol. 27 (2007) 1370–1379.
[29] C.L. Makino, I.V. Peshenko, X.H. Wen, E.V. Olshevskaya, R. Barrett, A.M. Dizhoor, A role for GCAP2 in regulating the photoresponse. Guanylyl cyclase activation and rod electrophysiology in GUCA1B knock-out mice, J. Biol. Chem. 283 (2008) 29135–29143.
[30] K.A. Howes, M.E. Pennesi, I. Sokal, J. Church-Kopish, B. Schmidt, D. Margolis, J.M. Frederick, F. Rieke, K. Palczewski, S.M. Wu, P.B. Detwiler, W. Baehr, GCAP1 rescues rod photoreceptor response in GCAP1/GCAP2 knockout mice, EMBO J. 21 (2002) 1545–1554.
[31] A. Mendez, M.E. Burns, I. Sokal, A.M. Dizhoor, W. Baehr, K. Palczewski, D.A. Baylor, J. Chen, Role of guanylate cyclase-activating proteins (GCAPs) in setting the flash sensitivity of rod photoreceptors, Proc. Natl. Acad. Sci. U. S. A. 98 (2001) 9948–9953.
[32] R.G. Collum, P.E. Fisher, M. Datta, S. Mellis, C. Thiele, K. Huebner, C.M. Croce, M.A. Israel, T. Theil, T. Moroy, R. DePinho, W.A. Alt, A novel POU homeodomain gene specifically expressed in cells of the developing mammalian nervous system, Nucleic Acids Res. 20 (1992) 4919–4925.
[33] M. Xiang, L. Zhou, J.P. Macke, T. Yoshioka, S.H. Hendry, R.L. Eddy, T.B. Shows, J. Nathans, The Brn-3 family of POU-domain factors: primary structure, binding specificity, and expression in subsets of retinal ganglion cells and somatosensory neurons, J. Neurosci. 15 (1995) 4762–4785.